Inorganic Chemistry

ARTICLE

pubs.acs.org/IC

Efficient Plasmid DNA Cleavage by Copper(II) Complexes of 1,4,7-Triazacyclononane Ligands Featuring Xylyl-Linked Guanidinium Groups

Linda Tjioe,[†] Anja Meininger,[†,‡] Tanmaya Joshi,[†] Leone Spiccia,[*,†] and Bim Graham[*,§]

[†]School of Chemistry, Monash University, Clayton, Victoria 3800, Australia

[§]Medicinal Chemistry and Drug Action, Monash Institute of Pharmaceutical Sciences, Monash University, Parkville, Victoria 3052, Australia

Supporting Information

ABSTRACT: Three new metal-coordinating ligands, $\mathbf{L^1}$, $\mathbf{L^2}$, and $\mathbf{L^3}$, have been prepared by appending *o*-, *m*-, and *p*-xylylguanidine pendants, respectively, to one of the nitrogen atoms of 1,4,7-triazacyclononane (tacn). The copper(II) complexes of these ligands are able to accelerate cleavage of the P−O bonds within the model phosphodiesters bis(*p*-nitrophenyl)phosphate (BNPP) and [2-(hydroxypropyl)-*p*-nitrophenyl]phosphate (HPNPP), as well as supercoiled pBR 322 plasmid DNA. Their reactivity toward BNPP and HPNPP is not significantly different from that of the nonguanidinylated analogues, $[Cu(tacn)(OH_2)_2]^{2+}$ and $[Cu(1\text{-benzyl-tacn})(OH_2)_2]^{2+}$, but they cleave plasmid DNA at considerably faster rates than either of these two complexes. The complex of $\mathbf{L^1}$, $[Cu(\mathbf{L^1}H^+)(OH_2)_2]^{3+}$, is the most active of the series, cleaving the supercoiled plasmid DNA (form I) to the relaxed circular form (form II) with a k_{obs} value of $(2.7 \pm 0.3) \times 10^{-4}\ s^{-1}$, which corresponds to a rate enhancement of 22- and 12-fold compared to those of $[Cu(tacn)(OH_2)_2]^{2+}$ and $[Cu(1\text{-benzyl-tacn})(OH_2)_2]^{2+}$, respectively. Because of the relatively fast rate of plasmid DNA cleavage, an observed rate constant of $(1.2 \pm 0.5) \times 10^{-5}\ s^{-1}$ for cleavage of form II DNA to form III was also able to be determined. The X-ray crystal structures of the copper(II) complexes of $\mathbf{L^1}$ and $\mathbf{L^3}$ show that the distorted square-pyramidal copper(II) coordination sphere is occupied by three nitrogen atoms from the tacn ring and two chloride ions. In both complexes, the protonated guanidinium pendants extend away from the metal and form hydrogen bonds with solvent molecules and counterions present in the crystal lattice. In the complex of $\mathbf{L^1}$, the distance between the guanidinium group and the copper(II) center is similar to that separating the adjacent phosphodiester groups in DNA (ca. 6 Å). The overall geometry of the complex is also such that if the guanidinium group were to form charge-assisted hydrogen-bonding interactions with a phosphodiester group, a metal-bound hydroxide would be well-positioned to affect the nucleophilic attack on the neighboring phosphodiester linkage. The enhanced reactivity of the complex of $\mathbf{L^1}$ at neutral pH appears to also be, in part, due to the relatively low pK_a of 6.4 for one of the coordinated water molecules.

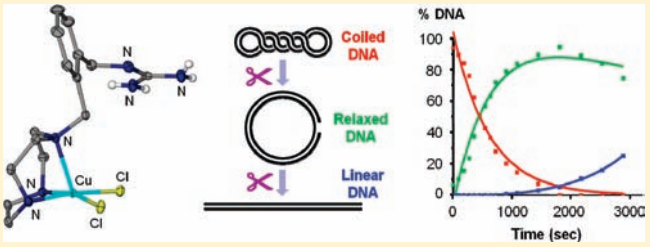

INTRODUCTION

Transition-metal complexes that are capable of cleaving the phosphate ester backbone of DNA and/or RNA under physiological conditions continue to be the subject of considerable research activity, spurred on by the prospect of producing tailormade artificial restriction enzymes and catalytic metallodrugs.[1−12] Despite significant advances, achieving practically useful rates of cleavage remains a major challenge. The P−O bonds within the sugar−phosphate backbone of nucleic acids are exceptionally resistant to hydrolytic cleavage because the negatively charged backbone strongly repels the attack of potential nucleophiles.[6] Nature spectacularly demonstrates, however, that it is possible to engineer molecules that can vastly reduce the activation energy associated with scission of these bonds. It has evolved a range of enzymes (nucleases, ribonucleases, and phosphatases) to facilitate manipulation of the phosphate esters on the subminute-to-second time scale.[13] Indeed, such enzymes are crucial to life, with reactions involving cleavage of the phosphodiesters or transfer of the phosphoryl groups underpinning many fundamental biological processes, e.g., cellular signaling and regulation, energy storage and production, and nucleic acid synthesis, degradation, and repair.[7,14−16] These enzymes have provided inspiration for the design of a large range of synthetic mimics. By the same token, our understanding of the relationship between enzyme structure and function has benefited considerably from the study of such model compounds.

A quite recent development in the field of artificial metallonucleases is the synthesis of metal complexes featuring ancillary

Received: November 18, 2010
Published: April 19, 2011

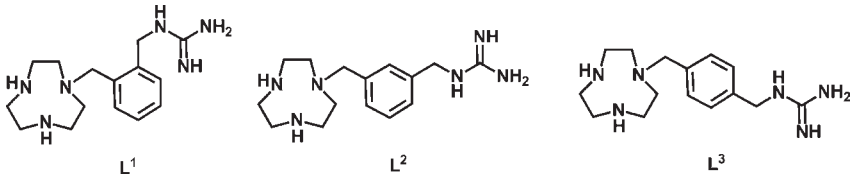

Figure 1. Ligands $\mathbf{L}^1$, $\mathbf{L}^2$, and $\mathbf{L}^3$ prepared in this study as tetrahydrochloride salts.

ammonium and guanidinium groups designed to mimic lysine and arginine residues found at the active sites of many metalloenzymes.[17−21] These charged residues complement the catalytic activity of metal ions by assisting with substrate binding and activation, as well as stabilization of the transition states.[22,23] The guanidinium-containing amino acid side chain of arginine, in particular, is frequently employed by enzymes to help bind anionic substrates.[22,24] It forms especially strong charge-assisted hydrogen bonds with phosphates and carboxylates.

Our most recent contribution to this area of research concerned the development of copper(II) complexes of 1,4,7-triazacyclononane (tacn) derivatives featuring two guanidine groups attached to the amines of the tacn ring via ethyl or propyl chains.[25] The complex incorporating propyl spacers was significantly more active in cleaving two model phosphodiesters, bis(*p*-nitrophenyl)phosphate (BNPP) and [2-(hydroxypropyl)-*p*-nitrophenyl]phosphate (HPNPP), than $[Cu(tacn)(OH_2)_2]^{2+}$ but only moderately more active than the copper(II) complexes of N-trialkylated tacn ligands. This suggested that the enhanced reactivity was largely due to, for example, the reduced formation of inactive dihydroxo-bridged dimers rather than the guanidine groups playing a major role in the cleavage mechanism. In addition, the complex was found to be only marginally more active in hydrolyzing plasmid DNA than $[Cu(tacn)(OH_2)_2]^{2+}$, possibly because of unfavorable steric interactions with the double-helix structure negating any potential positive contribution from the guanidine groups toward substrate binding and activation. Lastly, X-ray crystallography and speciation studies showed that, for the ligand with ethyl spacers, binding of the guanidine groups resulted in a very stable five-coordinate complex that was unreactive toward BNPP and HPNPP.

Taking the above findings into consideration, we postulated that better cleavage activity might be achieved with copper(II) complexes of tacn ligands featuring single guanidine groups attached via aromatic spacers. Our hypothesis was that more rigid pendants would enhance the activity by (i) preventing coordination of the guanidine group to the copper(II) center and (ii) reducing the entropic penalty associated with the simultaneous binding of the copper(II) center and protonated guanidinium group to the phosphodiester substrate, provided a spacer with suitable geometry could be found.[26,27] The incorporation of a single pendant, rather than two, should reduce the possibility of unfavorable steric interactions occurring upon attack of the complex on a double-helix structure. Herein, we describe the results of a study designed to test these hypotheses. This involved the preparation of copper(II) complexes of three new tacn-based ligands, $\mathbf{L}^1$, $\mathbf{L}^2$, and $\mathbf{L}^3$, featuring *o*-, *m*-, and *p*-xylylguanidine pendant groups, respectively (Figure 1), and an examination of the kinetics of cleavage of BNPP, HPNPP, and pBR 322 plasmid DNA by the three complexes. The crystal structures of the complexes of $\mathbf{L}^1$ and $\mathbf{L}^3$ were also determined, helping to shed some light on the reasons for the observed differences in the cleavage activity.

EXPERIMENTAL SECTION

Materials and Chemicals. Chemicals and solvents were of reagent or analytical grade, and were used as received unless otherwise indicated. Distilled water and high-performance liquid chromatography (HPLC)-grade chloroform were used throughout. Tetrahydrofuran (THF) was dried over 4 Å molecular sieves and then freshly distilled from sodium/benzophenone prior to use. 1,4-Bis(*tert*-butoxycarbonyl)-1,4,7-triazacyclononane[28] and the sodium salt of [2-(hydroxypropyl)-*p*-nitrophenyl]phosphate (NaHPNPP)[29,30] were prepared according to literature procedures. pBR 322 plasmid DNA was purchased from Promega Corp. Milli-Q water used for DNA cleavage was sterilized by autoclaving, and all reaction solutions were prepared according to standard sterile techniques. Deoxygenated water was prepared by boiling distilled water under nitrogen for 4 h and cooling while bubbling with nitrogen gas. High-purity nitrogen gas was used directly from a reticulated system.

Instrumentation and Methods. IR spectra were recorded as KBr disks using a Bruker Equinox FTIR spectrometer at 4.0 cm^{-1} resolution, fitted with an attenuated total reflectance (ATR) platform. Microanalyses were performed by Campbell Microanalytical Service, Otago, New Zealand. ^1H and ^{13}C NMR spectra were recorded at 25 °C in D_2O or $CDCl_3$ (as listed) on a Bruker AC200, AM300, or DX400 spectrometer. Chemical shifts were recorded on the δ scale in parts per million (ppm). The chemical shifts, δ, were calibrated using either tetramethylsilane or signals from the residual protons of deuterated solvents. Abbreviations for the resonances for ^1H NMR spectra are as follows: s (singlet), d (doublet), t (triplet), q (quartet), m (multiplet), and br s (broad singlet). Low-resolution electrospray ionization mass spectrometry (ESI-MS) spectra were obtained with a Micromass Platform II quadrupole mass spectrometer fitted with an electrospray source. The capillary voltage was at 3.5 eV and the cone voltage at 35 V. Thin-layer chromatography was performed using silica gel 60 F-254 (Merck) plates with detection of the species present by UV irradiation or $KMnO_4$ oxidation. UV−vis spectra were recorded in 1 cm quartz cuvettes using a Varian Cary Bio 300 or 5G spectrophotometer. Circular dichroism (CD) spectra of DNA were recorded at room temperature on a Jasco J-815 spectropolarimeter with a continuous flow of nitrogen purging the polarimeter, using 1-cm-path-length quartz cuvettes. Each sample solution was scanned from 320 to 220 nm at a speed of 20 nm min^{-1}, and the buffer background spectrum was automatically subtracted. Data were recorded at intervals of 0.1 nm. The CD spectrum of calf thymus DNA (CT-DNA) alone (116 μM) was recorded as a control, together with the CD spectra of DNA in the presence of the complex at various [complex]/[DNA] ratios (0.0, 0.1, 0.2, 0.4, 0.6, 0.8, 1.0, 1.5, 2.0, 2.5, 3.0, 3.5, and 4.0). Agarose gel electrophoresis of plasmid DNA cleavage products was performed using a Biorad Mini-Protean 3 electrophoresis module. Bands were visualized by UV light irradiation, fluorescence-imaged using an AlphaImager, and photographed with a CCD camera. The gel photographs were analyzed with the aid of the *ImageQuaNT* program, version 4.1.

Caution! *Although no problems were encountered in this work, perchlorate salts are potentially explosive. They should be prepared in small quantities and handled with care.*

dx.doi.org/10.1021/ic102301n |*Inorg. Chem.* 2011, 50, 4327–4339

Syntheses. *1-(o-Phthalimidoxylyl)-4,7-bis(tert-butoxycarbonyl)-1,4,7-triazacyclononane (**1**).* A solution of 2-[2-(bromomethyl)benzyl]-isoindoline-1,3-dione (2.89 g, 8.78 mmol) in acetonitrile (50 mL) was added dropwise to a mixture of 1,4-bis(*tert*-butoxycarbonyl)-1,4,7-triazacyclononane (2.89 g, 8.78 mmol), K_2CO_3 (3.03 g, 22.0 mmol), and KI (0.12 g) in acetonitrile (50 mL). The resulting mixture was stirred for 1 h at room temperature and then refluxed for 3 days. After cooling to room temperature, the inorganic salts were filtered off and the solvent was removed from the filtrate under reduced pressure to yield **1** as a yellow oil. Yield: 4.06 g (80%). ^{1}H NMR (300 MHz, $CDCl_3$): δ 1.43 (s, 18H, ^{t}Bu CH_3), 2.73 (m, 4H, tacn CH_2), 3.23−3.30 (m, 4H, tacn CH_2), 3.45−3.53 (m, 4H, tacn CH_2), 3.96 (s, 2H, ethyl CH_2), 5.07 (s, 2H, ethyl CH_2), 7.16−7.19 (m, 4H, aromatic CH), 7.70−7.73 (m, 2H, aromatic CH), 7.82−7.87 (m, 2H, aromatic CH). ^{13}C NMR (75 MHz, $CDCl_3$): δ 28.4 (^{t}Bu CH_3), 38.1 (ethyl CH_2), 47.8−54.7 (tacn CH_2), 59.8 (ethyl CH_2), 79.7 (quaternary ^{t}Bu C), 123.2, 127.4, 128.2, 130.5, 132.0, 133.9, 135.5, 137.1 (aromatic CH), 155.5 (C═O), 168.1 (C═O). IR (neat, cm^{-1}): 3058w ($\nu_{C-H(aromatic)}$), 2974s (ν_{C-H}), 1690s ($\nu_{C=O}$), 1682s ($\nu_{C=O}$), 1464s, 1393s, 1249s (ν_{C-O}), 1160s, 998w, 860w, 772w, 716w, 628w. ESI-MS: m/z 579.3 (100%) $[M + H]^+$.

*1-(m-Phthalimidoxylyl)-4,7-bis(tert-butoxycarbonyl)-1,4,7-triazacyclononane (**2**).* Compound **2** was prepared as a yellow oil in a manner identical with that of **1** by the slow addition of 2-[3-(bromomethyl)benzyl]isoindoline-1,3-dione (3.47 g, 10.5 mmol) in acetonitrile (50 mL) to a mixture of 1,4-bis(*tert*-butoxycarbonyl)-1,4,7-triazacyclononane (3.47 g, 10.5 mmol), K_2CO_3 (3.64 g, 26.4 mmol), and KI (0.12 g) in acetonitrile. Yield: 4.68 g (77%). ^{1}H NMR (300 MHz, $CDCl_3$): δ 1.40 (s, 18H, ^{t}Bu CH_3), 2.56−2.68 (m, 4H, tacn CH_2), 3.15−3.27 (m, 4H, tacn CH_2), 3.44−3.51 (m, 4H, tacn CH_2), 3.63 (s, 2H, ethyl CH_2), 4.80 (s, 2H, ethyl CH_2), 7.18−7.33 (m, 4H, aromatic CH), 7.68−7.71 (m, 2H, aromatic CH), 7.81−7.84 (m, 2H, aromatic CH). ^{13}C NMR (75 MHz, $CDCl_3$): δ 28.4 (^{t}Bu CH_3), 41.5 (ethyl CH_2), 49.2−53.8 (tacn CH_2), 60.6 (ethyl CH_2), 79.3 (quaternary ^{t}Bu C), 123.2, 126.9, 128.3, 128.5, 128.8, 132.0, 133.9, 136.1, 140.5 (aromatic CH), 155.6 (C═O), 167.8 (C═O). IR (neat, cm^{-1}): 3058w ($\nu_{C-H(aromatic)}$), 2974s (ν_{C-H}), 1686s ($\nu_{C=O}$), 1682s ($\nu_{C=O}$), 1466m, 1394s, 1248m (ν_{C-O}), 1158s, 955w, 859w, 772w, 712w, 530w. ESI-MS: m/z 579.3 (100%) $[M + H]^+$.

*1-(p-Phthalimidoxylyl)-4,7-bis(tert-butoxycarbonyl)-1,4,7-triazacyclononane (**3**).* Compound **3** was prepared as a yellow oil following the procedure described for **1** by the slow addition of 2-[4-(bromomethyl)-benzyl]isoindoline-1,3-dione (3.01 g, 9.15 mmol) in acetonitrile (50 mL) to a mixture of 1,4-bis(*tert*-butoxycarbonyl)-1,4,7-triazacyclononane (3.00 g, 9.15 mmol), K_2CO_3 (3.16 g, 22.9 mmol), and KI (0.12 g) in acetonitrile (50 mL). Yield: 4.03 g (76%). ^{1}H NMR (300 MHz, $CDCl_3$): δ 1.41 (s, 18H, ^{t}Bu CH_3), 2.47−2.64 (m, 4H, tacn CH_2), 3.10−3.31 (m, 4H, tacn CH_2), 3.42−3.46 (m, 4H, tacn CH_2), 3.56 (s, 2H, ethyl CH_2), 4.77 (s, 2H, ethyl CH_2), 7.17−7.34 (m, 4H, aromatic CH), 7.61−7.68 (m, 2H, aromatic CH), 7.75−7.80 (m, 2H, aromatic CH). ^{13}C NMR (75 MHz, $CDCl_3$): δ 28.4 (^{t}Bu CH_3), 41.1 (ethyl CH_2), 49.0−53.9 (tacn CH_2), 60.2 (ethyl CH_2), 79.3 (quaternary ^{t}Bu C), 123.1, 128.2, 129.1, 131.9, 133.7, 134.9, 139.5 (aromatic CH), 155.5 (C═O), 167.7 (C═O). IR (neat, cm^{-1}): 3057w ($\nu_{C-H(aromatic)}$), 2975s (ν_{C-H}), 1702s ($\nu_{C=O}$), 1687s ($\nu_{C=O}$), 1478s, 1393s, 1247s (ν_{C-O}), 1160s, 938w, 860w, 772w, 715s, 624w. ESI-MS: m/z 579.3 (100%) $[M + H]^+$.

*1-(o-Aminoxylyl)-4,7-bis(tert-butoxycarbonyl)-1,4,7-triazacyclononane (**4**).* Compound **1** (4.06 g, 7.01 mmol) was dissolved in ethanol (50 mL), and hydrazine monohydrate (2.45 g, 49.1 mmol) was added. The solution was heated at 50 °C for 4 h. The white precipitate that formed was removed by filtration. The filtrate was evaporated under reduced pressure, and the residue was treated with CH_2Cl_2 (50 mL). The organic layer was washed with 1 M NaOH (2 × 50 mL) and dried with Na_2SO_4, and the solvent was removed under vacuum to produce a yellow oil. Yield: 2.48 g (79%). ^{1}H NMR (300 MHz, $CDCl_3$): δ 1.46 (s, 18H, ^{t}Bu CH_3), 1.95 (s br, 2H, NH_2), 2.60−2.71 (m, 4H, tacn CH_2), 3.20−3.22 (m, 4H, tacn CH_2), 3.35−3.43 (m, 4H, tacn CH_2), 3.70 (s, 2H, ethyl CH_2), 3.83 (s, 2H, ethyl CH_2), 7.12−7.31 (m, 4H, aromatic CH). ^{13}C NMR (75 MHz, $CDCl_3$): δ 28.3 (^{t}Bu CH_3), 43.8 (ethyl CH_2), 48.2−53.3 (tacn CH_2), 58.7 (ethyl CH_2), 79.5 (quaternary ^{t}Bu C), 126.5, 127.4, 128.0, 130.3 (aromatic CH), 136.7, 142.1 (aromatic C), 155.4 (C═O). IR (neat, cm^{-1}): 3369w (ν_{N-H}), 2974s ($\nu_{C-H(aromatic)}$), 2864s (ν_{C-H}), 1694s ($\nu_{C=O}$), 1455s, 1416s, 1367s, 1247s (ν_{C-O}), 1170s, 1027m, 998s, 860s, 772s. ESI-MS: m/z 449.2 (100%) $[M + H]^+$.

*1-(m-Aminoxylyl)-4,7-bis(tert-butoxycarbonyl)-1,4,7-triazacyclononane (**5**).* Compound **5** was prepared following the same method as that for **4** but using **2** (4.68 g, 8.09 mmol) and hydrazine monohydrate (2.83 g, 56.7 mmol). Yield: 2.90 g (80%). ^{1}H NMR (300 MHz, $CDCl_3$): δ 1.45 (s, 18H, ^{t}Bu CH_3), 1.68 (s br, 2H, NH_2), 2.56−2.67 (m, 4H, tacn CH_2), 3.10−3.26 (m, 4H, tacn CH_2), 3.39−3.48 (m, 4H, tacn CH_2), 3.60 (s, 2H, ethyl CH_2), 3.78 (s, 2H, ethyl CH_2), 7.10−7.21 (m, 4H, aromatic CH). ^{13}C NMR (75 MHz, $CDCl_3$): δ 28.4 (^{t}Bu CH_3), 46.3 (ethyl CH_2), 48.8−54.1 (tacn CH_2), 60.8 (ethyl CH_2), 79.3 (quaternary ^{t}Bu C), 125.5, 127.3, 127.5, 128.2 (aromatic CH), 140.1, 143.0 (aromatic C), 155.5 (C═O). IR (neat, cm^{-1}): 3375w (ν_{N-H}), 2974s ($\nu_{C-H(aromatic)}$), 2862s (ν_{C-H}), 1694s ($\nu_{C=O}$), 1455s, 1416s, 1360s, 1250s (ν_{C-O}), 1155s, 1095m, 978s, 831s, 772s. ESI-MS: m/z 449.2 (100%) $[M + H]^+$.

*1-(p-Aminoxylyl)-4,7-bis(tert-butoxycarbonyl)-1,4,7-triazacyclononane (**6**).* Compound **6** was prepared via the method used to obtain **4** but using **3** (4.03 g, 6.97 mmol) and hydrazine monohydrate (2.44 g, 48.8 mmol). Yield: 2.48 g (79%). ^{1}H NMR (300 MHz, $CDCl_3$): δ 1.45 (s, 18H, ^{t}Bu CH_3), 1.54 (s br, 2H, NH_2), 2.55−2.66 (m, 4H, tacn CH_2), 3.10−3.25 (m, 4H, tacn CH_2), 3.39−3.47 (m, 4H, tacn CH_2), 3.59 (s, 2H, ethyl CH_2), 3.78 (s, 2H, ethyl CH_2), 7.12−7.28 (m, 4H, aromatic CH). ^{13}C NMR (75 MHz, $CDCl_3$): δ 28.3 (^{t}Bu CH_3), 46.0 (ethyl CH_2), 48.7−53.9 (tacn CH_2), 60.4 (ethyl CH_2), 79.3 (quaternary ^{t}Bu C), 126.6, 129.0 (aromatic CH), 138.3, 142.1 (aromatic C), 155.5 (C═O). IR (neat, cm^{-1}): 3373w (ν_{N-H}), 2975s ($\nu_{C-H(aromatic)}$), 2864s (ν_{C-H}), 1694s ($\nu_{C=O}$), 1463s, 1415s, 1366s, 1248s (ν_{C-O}), 1160s, 1092w, 979w, 860w, 772w. ESI-MS: m/z 449.2 (100%) $[M + H]^+$.

*1-{o-[bis(tert-Butoxycarbonyl)guanidino]xylyl}-4,7-bis(tert-butoxycarbonyl)-1,4,7-triazacyclononane (**7**).* To a stirred solution of **4** (2.48 g, 5.53 mmol) in THF (20 mL) was added *N,N′*-Boc_2-1*H*-pyrazole-1-carboxamidine (1.72 g, 5.53 mmol) in THF (20 mL). The resulting solution was stirred at room temperature for 2 days. The solvent was evaporated under reduced pressure, and the residue was dissolved with CH_2Cl_2 (50 mL). The organic layer was then washed with 0.1 M NaOH (3 × 30 mL) and dried with Na_2SO_4, and the solvent was removed under vacuum to produce a yellow oil. The crude product was purified by silica gel column chromatography using 2% MeOH/$CHCl_3$ as the eluent. R_f = 0.25. Yield: 3.02 g (79%). ^{1}H NMR (300 MHz, $CDCl_3$): δ 1.32 (s, 9H, ^{t}Bu CH_3), 1.39 (s, 27H, ^{t}Bu CH_3), 2.56−2.61 (m, 4H, tacn CH_2), 3.15 (m, 4H, tacn CH_2), 3.32−3.45 (m, 4H, tacn CH_2), 3.65 (s, 2H, ethyl CH_2), 4.70 (m. 2H, ethyl CH_2), 7.11−7.43 (m, 4H, aromatic CH), 8.45 (t br, NHBoc). ^{13}C NMR (75 MHz, $CDCl_3$): δ 27.9 (^{t}Bu CH_3), 28.2 (^{t}Bu CH_3), 28.4 (^{t}Bu CH_3), 42.4 (ethyl CH_2), 48.3−54.5 (TACN CH_2), 59.5 (ethyl CH_2), 79.2 (quaternary ^{t}Bu C), 79.4 (quaternary ^{t}Bu C), 82.9 (quaternary ^{t}Bu C), 127.4 (aromatic CH), 128.5, 130.3 (aromatic CH), 136.2, 137.2 (aromatic C), 153.0 (C═O), 155.9 (C═O), 163.5 (C═O). IR (neat, cm^{-1}): 3334s (ν_{N-H}), 3138m (ν_{N-H}), 2978s ($\nu_{C-H(aromatic)}$), 1716s ($\nu_{C=O}$), 1683s ($\nu_{C=O}$), 1634s ($\nu_{C=O}$), 1557s ($\nu_{C=N}$), 1456s, 1250s (ν_{C-O}), 1157s, 1058s, 999w, 927w, 869w. ESI-MS: m/z 691.4 (100%) $[M + H]^+$.

*1-{m-[bis(tert-Butoxycarbonyl)guanidino]xylyl}-4,7-bis(tert-butoxycarbonyl)-1,4,7-triazacyclononane (**8**).* Compound **8** was prepared via the method to obtain **7**, by reacting **5** (2.90 g, 6.47 mmol) with *N,N′*-Boc_2-1*H*-pyrazole-1-carboxamidine (2.01 g, 6.47 mmol). Yield: 3.48 g (78%). ^{1}H NMR (300 MHz, $CDCl_3$): δ 1.43 (s, 9H, ^{t}Bu CH_3), 1.49

(s, 27H, ^{t}Bu CH_3), 2.63−2.71 (m, 4H, tacn CH_2), 3.16−3.30 (m, 4H, tacn CH_2), 3.44−3.52 (m, 4H, tacn CH_2), 3.66 (s, 2H, ethyl CH_2), 4.60 (m, 2H, ethyl CH_2), 7.15−7.34 (m, 4H, aromatic CH), 8.53 (t br, NHBoc). ^{13}C NMR (75 MHz, $CDCl_3$): δ 28.2 (^{t}Bu CH_3), 28.6 (^{t}Bu CH_3), 28.8 (^{t}Bu CH_3), 45.2 (ethyl CH_2), 49.4−54.8 (tacn CH_2), 60.9 (ethyl CH_2), 79.5 (quaternary ^{t}Bu C), 79.7 (quaternary ^{t}Bu C), 83.3 (quaternary ^{t}Bu C), 126.6 (aromatic CH), 128.5 (aromatic CH), 128.9 (aromatic CH), 137.3, 140.8 (aromatic C), 153.2 (C═O), 156.2 (C═O), 163.8 (C═O). IR (neat, cm^{-1}): 3336s (ν_{N-H}), 3140m (ν_{N-H}), 2978s ($\nu_{C-H(aromatic)}$), 1720s ($\nu_{C=O}$), 1694s ($\nu_{C=O}$), 1639s ($\nu_{C=O}$), 1570s ($\nu_{C=N}$), 1478s, 1250s (ν_{C-O}), 1157s, 1058s, 980w, 913w, 858w. ESI-MS: m/z 691.4 (100%) $[M + H]^+$.

*1-{p-[bis(tert-Butoxycarbonyl)guanidino]xylyl}-4,7-bis(tert-butoxycarbonyl)-1,4,7-triazacyclononane (**9**).* Compound **9** was prepared in a manner identical with that of **7**, by reacting precursor **6** (2.48 g, 5.53 mmol) with *N,N′*-Boc_2-1*H*-pyrazole-1-carboxamidine (1.72 g, 5.53 mmol). Yield: 2.91 g (76%). ^{1}H NMR (300 MHz, $CDCl_3$): δ 1.40 (s, 9H, ^{t}Bu CH_3), 1.47 (s, 27H, ^{t}Bu CH_3), 2.62−2.65 (m, 4H, tacn CH_2), 3.13−3.28 (m, 4H, tacn CH_2), 3.40−3.49 (m, 4H, tacn CH_2), 3.60 (m, 2H, ethyl CH_2), 4.56 (m, 2H, ethyl CH_2), 7.16−7.54 (m, 4H, aromatic CH), 8.52 (t br, NHBoc). ^{13}C NMR (75 MHz, $CDCl_3$): δ 28.0 (^{t}Bu CH_3), 28.2 (^{t}Bu CH_3), 28.5 (^{t}Bu CH_3), 44.7 (ethyl CH_2), 48.2−54.3 (tacn CH_2), 60.4 (ethyl CH_2), 79.2 (quaternary ^{t}Bu C), 79.5 (quaternary ^{t}Bu C), 83.0 (quaternary ^{t}Bu C), 127.4 (aromatic CH), 128.9 (aromatic CH), 129.2 (aromatic CH), 135.8, 139.4 (aromatic C), 153.0 (C═O), 155.6 (C═O), 163.5 (C═O). IR (neat, cm^{-1}): 3336s (ν_{N-H}), 3138m (ν_{N-H}), 2978s ($\nu_{C-H(aromatic)}$), 1722s ($\nu_{C=O}$), 1683s ($\nu_{C=O}$), 1640s ($\nu_{C=O}$), 1557s ($\nu_{C=N}$), 1458s, 1250s (ν_{C-O}), 1158s, 1058s, 1000w, 927w, 869w. ESI-MS: m/z 691.4 (90%) $[M + H]^+$, 713.4 (10%) $[M + Na]^+$.

*1-(o-Guanidinoxylyl)-1,4,7-triazacyclononane Tetrahydrochloride (**L^1**·4HCl).* A solution of the Boc-protected amine **7** (3.02 g, 4.37 mmol) was dissolved in a mixture of 1:1 (v/v) TFA/CH_2Cl_2 (10 mL) and the solution stirred at room temperature overnight. The solvent was then removed under reduced pressure and the residual brown oil dissolved in a mixture of EtOH (5 mL) and concentrated HCl (2 mL). The addition of diethyl ether (5 mL) produced a white precipitate, which was filtered, dissolved in a small amount of distilled water, and then freeze-dried to yield the product as a white solid. Yield: 0.87 g (68%). Microanal. Calcd for $C_{15}H_{36}N_6Cl_4$: C, 35.9; H, 7.3; N, 16.8; Cl, 30.4. Found: C, 36.0; H, 7.0; N, 16.7; Cl, 30.7. ^{1}H NMR (300 MHz, D_2O): δ 3.11−3.14 (m, 4H, tacn CH_2), 3.30−3.33 (m, 4H, tacn CH_2), 3.75 (s, 4H, tacn CH_2), 4.00 (s, 2H, ethyl CH_2), 4.54 (s, 2H, ethyl CH_2), 7.44−7.61 (m, 4H, aromatic CH). ^{13}C NMR (75 MHz, D_2O): δ 43.0 (tacn CH_2), 43.1 (ethyl CH_2), 44.7 (tacn CH_2), 49.2 (tacn CH_2), 56.1 (ethyl CH_2), 128.9 (aromatic CH), 129.1 (aromatic CH), 131.3 (aromatic CH), 134.8 (aromatic C), 134.9 (aromatic C), 157.1 (C═N). IR (KBr disk, cm^{-1}): 3334s (ν_{N-H}), 2986s ($\nu_{C-H(aromatic)}$), 2960s (ν_{C-H}), 1678s ($\nu_{C=N}$), 1450m, 1263w, 1107w, 980w. ESI-MS: m/z 291.3 (100%) $[M + H]^+$.

*1-(m-Guanidinoxylyl)-1,4,7-triazacyclononane Tetrahydrochloride (**L^2**·4HCl).* Deprotection of compound **8** (3.48 g, 5.04 mmol) following the procedure described for **L^1**·4HCl yielded the product as a white solid. Yield: 0.98 g (67%). Microanal. Calcd for $C_{15}H_{36}N_6Cl_4$: C, 36.1; H, 7.3; N, 16.8; Cl, 30.2. Found: C, 36.1; H, 6.8; N, 16.7; Cl, 30.5. ^{1}H NMR (300 MHz, D_2O): δ 3.06−3.10 (m, 4H, tacn CH_2), 3.26−3.29 (m, 4H, tacn CH_2), 3.68 (s, 4H, tacn CH_2), 3.97 (s, 2H, ethyl CH_2), 4.49 (s, 2H, ethyl CH_2), 7.38−7.53 (m, 4H, aromatic CH). ^{13}C NMR (75 MHz, D_2O): δ 42.6 (tacn CH_2), 44.0 (tacn CH_2), 44.7 (ethyl CH_2), 48.0 (tacn CH_2), 59.2 (ethyl CH_2), 127.2 (aromatic CH), 128.9 (aromatic CH), 129.7 (aromatic CH), 130.1 (aromatic CH), 136.2 (aromatic C), 137.1 (aromatic C), 157.2 (C═N). IR (KBr disk, cm^{-1}): 3338s (ν_{N-H}), 2986s ($\nu_{C-H(aromatic)}$), 2960s (ν_{C-H}), 1619s ($\nu_{C=N}$), 1450m, 1263w, 1110w, 954w. ESI-MS: m/z 291.3 (100%) $[M + H]^+$.

*1-(p-Guanidinoxylyl)-1,4,7-triazacyclononane Tetrahydrochloride (**L^3**·4HCl).* Deprotection of **9** (2.91 g, 4.21 mmol), as for the synthesis of **L^1**·4HCl, yielded the product as a yellow solid. Yield: 0.85 g (70%). Microanal. Calcd for $C_{15}H_{37}N_6Cl_5$: C, 34.2; H, 7.1; N, 16.0; Cl, 33.7. Found C, 34.5; H, 6.8; N, 15.7; Cl, 33.2. ^{1}H NMR (300 MHz, D_2O): δ 2.95−2.98 (m, 4H, tacn CH_2), 3.14−3.17 (m, 4H, tacn CH_2), 3.55 (s, 4H, tacn CH_2), 3.84 (s, 2H, ethyl CH_2), 4.35 (s, 2H, ethyl CH_2), 7.29−7.38 (m, 4H, aromatic CH). ^{13}C NMR (75 MHz, D_2O): δ 42.5 (tacn CH_2), 43.9 (tacn CH_2), 44.5 (ethyl CH_2), 48.1 (tacn CH_2), 59.0 (ethyl CH_2), 127.7 (aromatic CH), 131.1 (aromatic CH), 135.1 (aromatic C), 136.5 (aromatic C), 157.2 (C═N). IR (KBr disk, cm^{-1}): 3403s (ν_{N-H}), 2983s ($\nu_{C-H(aromatic)}$), 2960s (ν_{C-H}), 1678s ($\nu_{C=N}$), 1450m, 1263w, 1107w, 980w. ESI-MS: m/z 291.3 (100%) $[M + H]^+$.

*[Cu(**L^1**H$^+$)Cl$_2$]Cl·0.25DMF·0.25Et$_2$O·1.5H$_2$O (**C1**).* To a stirred aqueous solution of **L^1**·4HCl (0.096 g, 0.19 mmol) (4 mL) was added $Cu(ClO_4)_2 \cdot 6H_2O$ (0.084 g, 0.23 mmol) dissolved in water (4 mL). The pH of the solution was adjusted to 9 with 1 M NaOH, resulting in a deepening of the blue color and precipitation of a small amount of $Cu(OH)_2$, which was removed by filtration. The solution was evaporated to dryness and the residue redissolved in *N,N′*-dimethylformamide (DMF). The slow diffusion of diethyl ether into this solution produced blue crystals of the product. Yield: 0.036 g (38%). Microanal. Calcd for $Cu_1C_{17}H_{34}Cl_3N_6O_2$: C, 38.3; H, 6.6; N, 16.7. Found: C, 38.4; H, 6.3; N, 16.5. UV−vis (H_2O): λ_{max} (nm) [ε_{max} (M^{-1} cm^{-1})]: 613 [69], 926 [24]. Selected IR bands (ATR, cm^{-1}): 3251s (ν_{N-H}), 3151s, 2939m (ν_{C-H}), 1638m ($\nu_{C=N}$), 1488w, 1089w, 1006w, 940w, 727w.

*[Cu(**L^2**H$^+$)Cl$_2$]Cl (**C2**).* Attempts to crystallize this complex from solutions of equimolar amounts of **L^2** and $Cu(ClO_4)_2 \cdot 6H_2O$ using different crystallization techniques were unsuccessful. The copper(II) complex solution of **C2** was prepared in situ by mixing equimolar amounts of the desired ligand and $Cu(ClO_4)_2 \cdot 6H_2O$ in water and adjusting the pH to 7 with the addition of NaOH. UV−vis (H_2O): λ_{max} (nm) [ε_{max} (M^{-1} cm^{-1})]: 630 [59], 987 [20].

*[Cu(**L^3**H$^+$)Cl$_2$]Cl·0.25MeOH·1.5H$_2$O (**C3**).* As for **C1**, **L^3**·4HCl (0.076 g, 0.14 mmol) (4 mL) was reacted with $Cu(ClO_4)_2 \cdot 6H_2O$ (0.064 g, 0.17 mmol) dissolved in water (4 mL). The product obtained by evaporation of the filtrate was dissolved in methanol. Diffusion of diethyl ether into this solution crystallized the product. Yield: 0.016 g (22%). Microanal. Calcd for $Cu_1C_{15}H_{31}Cl_3N_6O_2$: C, 36.9; H, 6.3; N, 16.9. Found: C, 36.6; H, 5.8; N, 16.7. UV−vis (H_2O): λ_{max} (nm) [ε_{max} (M^{-1} cm^{-1})]: 618 [64], 926 [20]. Selected IR bands (ATR, cm^{-1}): 3241s (ν_{N-H}), 2931m (ν_{C-H}), 1641m ($\nu_{C=N}$), 1487w, 1352w, 1152w, 1002w, 942w, 824w.

Solution Speciation Studies. pH titrations of **C1**−**C3** were performed by adding 1 μL aliquots of 10 M HCl to solutions of each complex ([complex] = 7.5 mM, total volume = 10 mL). Stock complex solutions were prepared by mixing equimolar amounts of the desired ligands and $Cu(ClO_4)_2 \cdot 6H_2O$ in water and adjusting the pH to 12 using 5 M NaOH. The solutions were stirred for 1 min after each addition to ensure that the pH was stable, and the background-corrected UV−vis−NIR spectrum was measured. The apparent pK_a values of the coordinated water molecules in **C1**−**C3** were determined experimentally from variation in the absorbance with $[H^+]$ at selected wavelengths of maximum change (625, 900, and 1000 nm). Variation in the absorbance versus $[H^+]$ over the pH range 4.0−8.0 was fitted using an equation derived assuming a single deprotonation/protonation process (deprotonation of a coordinated water molecule) occurring in the pH range of study:

$$[Cu(LH)(OH_2)^{2+}] \overset{K_a}{\rightleftharpoons} [Cu(LH)(OH_2)(OH)]^+ + H^+$$

The K_a value was determined by fitting the data to the equation $Abs = [Cu]_{total}[\varepsilon_{Cu} + \varepsilon_{Cu-OH}(K_a/H^+)]/[1 + (K_a/H^+)]$, where

dx.doi.org/10.1021/ic102301n |*Inorg. Chem.* 2011, 50, 4327–4339

Scheme 1. Synthesis of Hydrochloride Salts of Ligands L^1, L^2, and L^3[a]

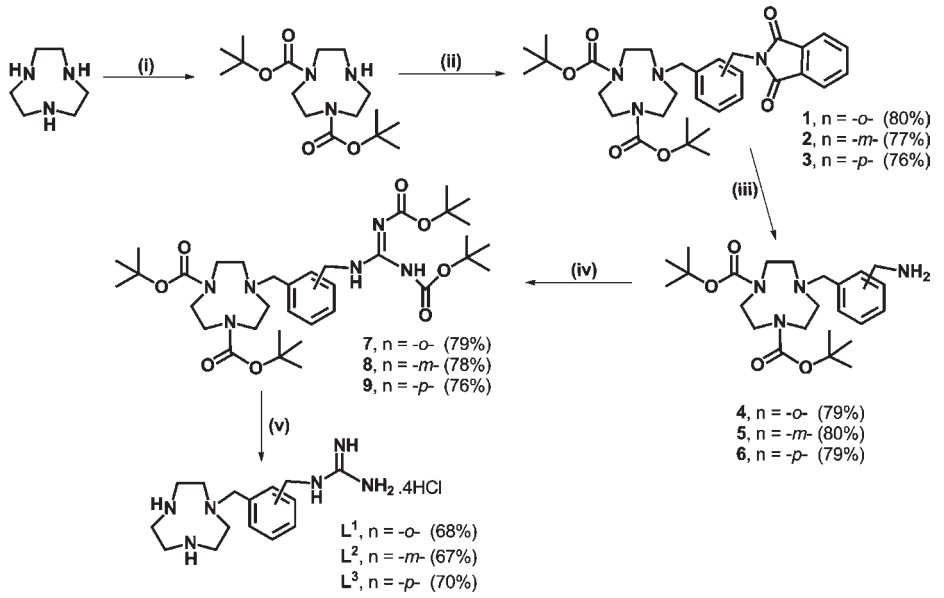

[a] (i) 2 equiv of Boc-ON, NEt_3, $CHCl_3$, RT, 8 h; (ii) *o*-, *m*-, or *p*-bromoxylylphthalimide, K_2CO_3, KI, CH_3CN, reflux, 3 days; (iii) $N_2H_4.H_2O$, EtOH, 50 °C, 4 h; (iv) *N,N′*-Boc_2-1*H*-pyrazole-1-carboxamidine, THF, RT, 2 days; (v) (a) 1:1 TFA/CH_2Cl_2, RT, o/n, (b) concentrated HCl.

Abs = absorbance at a particular wavelength, $[Cu]_{total}$ = total copper(II) complex concentration, and ε_{Cu} and ε_{Cu-OH} = molar extinction coefficients for the initial and monoprotonated copper(II) complexes, respectively. The choice of the model was supported by the fact that this equation fitted the experimental data extremely well.

Cleavage of Model Phosphate Esters. *Bis(p-nitrophenyl)-phosphate (BNPP).* These experiments were conducted using established procedures.[31,32] Briefly, the rate of cleavage of BNPP by the copper(II) complexes was measured at pH 7.0 (HEPES buffer) and pH 9.0 (CHES buffer) and T = 50 °C, by following the formation of a *p*-nitrophenoxide ion spectrophotometrically (λ_{max} = 400 nm, ε = 18 700 M^{-1} cm^{-1}) in solutions containing 0.1 mM BNPP, 2 mM copper(II) complex, and 0.15 M $NaClO_4$, over a period of 8000 min, with a reading taken every 5 min. Because the complex was in large excess compared to BNPP, the appearance of NP (and cleavage of BNPP) followed a first-order dependence. Observed rate constants were determined by fitting the data to the equation $Abs = A + Be^{-k_{obs}t}$.

[2-(Hydroxypropyl)-p-nitrophenyl]phosphate (HPNPP). These experiments were carried out in a manner similar to that of the BNPP experiments. The rate of cleavage of HPNPP by the copper(II) complexes was measured at pH 6.0 (MES), 7.0 (HEPES), and pH 9.0 (CHES) and T = 25 °C, in solutions containing 0.1 mM HPNPP, 2 mM copper(II) complex, and 0.15 M $NaClO_4$. The observed rate constants were determined as indicated above.

DNA Binding Assays. The binding of complexes **C1**−**C3** to CT-DNA was studied by CD spectroscopy. The measurements were performed at pH 7.0 and T = 20 °C, using 116 μM solutions of CT-DNA and increasing [complex]/[DNA] ratios (0.0, 0.1, 0.2, 0.4, 0.6, 0.8, 1.0, 1.5, 2.0, 2.5, 3.0, 3.5, and 4.0) dissolved in a 5 mM Tris-HCl/50 mM NaCl buffer. UV−vis spectrophotometry could not be used to monitor the interaction between small molecules and nucleic acids because these complexes absorb in regions similar to those of CT-DNA at 260 nm. The apparent binding constant, K_b, was determined from variation in the differential absorbance with [complex], using the equation $\Delta Abs = \{\Delta A_1 + \Delta A_2 K_b[Cu]\}/\{1 + K_b[Cu]\}$, where ΔA_1 and ΔA_2 are the differential absorbances with no complex added and with complex fully bound to DNA, respectively. The differential absorbance was obtained using the relationship $\Delta Abs = \theta/32.982$, where θ = degrees of ellipticity.

DNA Cleavage Experiments. Electrophoresis experiments were performed using pBR 322 plasmid DNA according the established procedures.[25] The cleavage of pBR 322 supercoiled plasmid DNA (38 μM base pair concentration) was accomplished by the addition of copper(II) complexes (75, 112.5, 150, 225, and 300 μM) dissolved in a 40 mM buffer (HEPES) at pH 7.0. The mixtures were incubated in a water bath at 37 °C for periods of up to 48 h. The reactions were quenched and the resulting solutions stored at −20 °C until just prior to analysis. The analysis involved loading of the solutions onto 1% agarose gels containing 1.0 μg dm^{-3} ethidium bromide, and the DNA fragments separated by gel electrophoresis (70 V for 2 h in standard Tris-acetate-EDTA (TAE) buffer, pH 8). Ethidium-stained agarose gels were imaged, and densitometric analysis of the visualized bands was used to determine the extent of supercoiled DNA cleavage, as reported in the literature.[17]

For all of the complexes except **C1**, the DNA cleavage data were fit to a first-order expression, $\%DNA = A + Be^{-k_{obs}t}$, yielding the first-order rate constant, k_{obs}, for cleavage of form I DNA to produce form II. In the case of **C1**, kinetic profiles were fitted using a single-strand cleavage model derived by Kishikawa et al.,[33] which accounts for not only conversion of form I to form II (rate constant k_1) but also subsequent nicking of form II to produce form III (rate constant k_2) and further cleavage of form III to produce undetected forms of DNA (rate constant k_3 represents all processes that cleave form III DNA). The rate equations for this model are as follows:

$$\frac{d[I]}{dt} = -k_1[I]; \quad \frac{d[II]}{dt} = k_1[I] - k_2[II]; \quad \frac{d[III]}{dt} = k_2[II] - k_3[III]$$

Integrating these expressions yields

$$[I] = C_0 e^{-k_1 t}$$
$$[II] = \frac{k_1 C_0}{k_2 - k_1} e^{-k_1 t} + \left(N_0 - \frac{k_1 C_0}{k_2 - k_1}\right) e^{-k_2 t}$$
$$[III] = \alpha e^{-k_1 t} + \beta e^{-k_2 t} + (L_0 - \alpha - \beta) e^{-k_3 t}$$

dx.doi.org/10.1021/ic102301n |*Inorg. Chem.* 2011, 50, 4327–4339

where $\alpha = k_1k_2C_0(k_2 - k_1)^{-1}(k_3 - k_1)^{-1}$ and

$$\beta = \left(\frac{-k_1C_0}{k_2 - k_1} + N_0\right)(k_3 - k_2)^{-1}$$

where C_0, N_0, and L_0 are the initial values of [I], [II], and [III], respectively.

Cleavage of pBR 322 plasmid DNA was also carried out in the presence of standard radical scavengers. Aliquots (5 μL) of aqueous solutions of scavenging agents (30 mM KI, DMSO, ^{t}BuOH, or NaN_3 in a 40 mM HEPES buffer at pH 7.0) were added to solutions of supercoiled DNA (5 μL, 113.5 μM base-pair concentration) prior to the addition of complexes **C1**, **C2**, and **C3**. The reaction conditions were 150 μM copper(II) complex, 10 mM scavenging agents, and 38 μM base-pair concentration for supercoiled plasmid DNA. Each solution was incubated at 37 °C for 6 h, quenched, and analyzed according to the procedure described above.

Experiments under anaerobic conditions were performed following the protocol reported by Hegg and Burstyn[34] and our previous work.[25] The concentrations for the reaction mixtures were 150 μM for complexes, 40 mM HEPES buffer, and 38 μM base-pair concentration for supercoiled DNA.

For complex **C1**, DNA cleavage experiments were also conducted using a fixed complex concentration of 50 μM and varying the concentration of pBR 322 plasmid DNA (base-pair concentration of 25−200 μM) at pH 7.0 (40 mM HEPES) and T = 37 °C.

The ionic strength dependence of the DNA cleavage activity of complex **C1** was evaluated over a range of NaCl concentrations (0, 20, 100, 250, and 500 mM). DNA cleavage experiments were performed with a 38 μM base-pair concentration of pBR 322 plasmid DNA and 150 μM copper(II) complex in a 40 mM HEPES buffer at pH 7.0 and T = 37 °C .

X-ray Crystallography. The intensity data for blue crystals of **C1** (0.20 × 0.20 × 0.05 mm) and **C3** (0.35 × 0.25 × 0.10 mm) were measured at 123 K on a Bruker Apex II CCD fitted with graphite-monochromated Mo Kα radiation (0.710 73 Å). The data were collected to a maximum 2θ value of 55° (60° for **C3**) and processed using the Bruker Apex II software package. The crystal parameters and details of the data collection are summarized in Table S01 in the Supporting Information. Each structure was solved by direct methods and expanded using standard Fourier routines in *SHELX-97*.[35,36] All hydrogen atoms were placed and refined in idealized positions, except for the hydrogen atoms on the nitrogen atoms, which were located on the Fourier difference map. All non-hydrogen atoms were refined anisotropically.

RESULTS AND DISCUSSION

Syntheses. The three new tacn ligand derivatives, L^1, L^2, and L^3, featuring xylylguanidine pendants, were prepared as their tetrahydrochloride salts following the route shown in Scheme 1. Following conversion of tacn to its di-Boc-protected derivative,[28] the remaining free nitrogen was functionalized by reaction with *o*-, *m*-, or *p*-bromoxylylphthalimide. Removal of the phthalimide protecting group with hydrazine then exposed an amine group within the newly introduced pendant, which was subsequently converted to a Boc-protected guanidine via treatment with *N*,*N*′-Boc$_2$-1*H*-pyrazole-1-carboxamidine. Global Boc deprotection using trifluoroacetic acid (TFA) yielded the target ligands, which were isolated as their tetrahydrochloride salts. The new compounds were characterized by ^{1}H and ^{13}C NMR spectroscopy, ESI-MS spectrometry, IR spectroscopy, and microanalysis.

The copper(II) complexes of L^1, **C1**, and L^3, **C3**, were crystallized by diffusion of diethyl ether into either DMF or methanolic solutions of the ligand and $Cu(ClO_4)_2 \cdot 6H_2O$, which had been adjusted to pH 9. Microanalytical data were consistent with the proposed formulas, and the IR spectra of the complexes showed bands due to the NH stretches of the guanidine group in the region of 3150−3250 cm^{-1}, as well as sharp bands in the range of 1640−1640 cm^{-1}, attributable to the ν(C═N) bands of the guanidine pendant groups. The electronic spectra of **C1** and **C3** exhibited broad absorption bands centered at 600 and 985 nm, typical for copper(II) complexes with square-pyramidal (SP) geometry.[37] Attempts to isolate the copper(II) complex of ligand L^2 from solution were unsuccessful. The UV−vis spectrum of this complex also exhibited bands indicative of a SP copper(II) geometry.

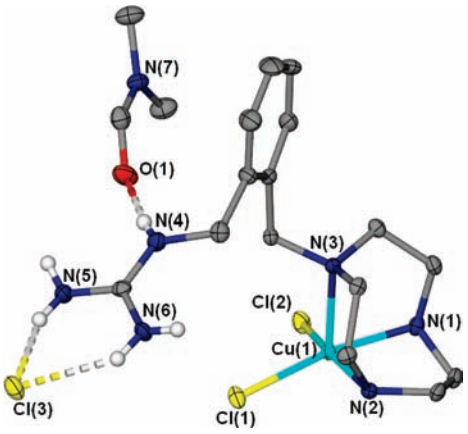

Figure 2. Thermal ellipsoid representation of the complex unit in **C1** showing the distorted SP copper(II) geometry and the hydrogen-bonding interactions formed by the charged guanidinium group (ellipsoids drawn at 50% probability; hydrogen atoms on carbon atoms and solvent molecules have been omitted for clarity).

Table 1. Selected Bond Lengths [Å] and Angles [deg] for C1

Cu(1)−N(1)	2.033(2)	N(2)−Cu(1)−N(1)	83.1(1)
Cu(1)−N(2)	2.037(2)	N(1)−Cu(1)−Cl(2)	88.42(7)
Cu(1)−N(3)	2.273(2)	N(2)−Cu(1)−Cl(2)	165.61(7)
Cu(1)−Cl(1)	2.2936(8)	N(1)−Cu(1)−N(3)	82.04(9)
Cu(1)−Cl(2)	2.2637(8)	N(2)−Cu(1)−N(3)	82.02(9)
		Cl(2)−Cu(1)−N(3)	108.33(6)
		N(1)−Cu(1)−Cl(1)	169.99(8)
		N(2)−Cu(1)−Cl(1)	90.20(7)
		Cl(2)−Cu(1)−Cl(1)	96.63(3)
		N(3)−Cu(1)−Cl(1)	104.40(6)

Crystallography. The crystal structures of complexes **C1** and **C3** were determined to ascertain the coordination environment of the copper(II) centers and the relative orientations of the guanidinium pendants.

Complex ***C1***. The molecular structure of **C1** consists of $[Cu(L^1H^+)Cl_2]^+$ cationic units (Figure 2), noncoordinated chloride anions, DMF, ether, and water molecules. The copper(II) center resides in a distorted SP geometry, with the basal planes defined by the two chlorine atoms and two secondary nitrogen atoms, N(1) and N(2), from the tacn macrocycle. The apical position is occupied by the tertiary nitrogen atom, N(3), bearing the protonated *o*-xylylguanidinium pendant. The degree of distortion (τ) from the ideal SP geometry to the trigonal-bipyramidal (TBP) geometry can be defined as a function of the two largest basal angles, θ and Φ: $\tau = [(\theta - \Phi)/60)] \times 100$, with τ = 0% for the ideal

dx.doi.org/10.1021/ic102301n |*Inorg. Chem.* 2011, 50, 4327–4339

Table 2. Hydrogen-Bonding Interactions in C1 [Å and deg][a]

D−H···A	d(D−H)	d(H···A)	d(D···A)	∠DHA
N(2)−H(2N)···Cl(2)#1	0.86(4)	2.62(4)	3.303(3)	137(3)
N(4)−H(4N)···O(1)#2	0.74(4)	2.00(4)	2.731(3)	168(4)
N(6)−H(6AN)···Cl(3)#3	0.87(4)	2.43(4)	3.224(3)	151(3)
N(6)−H(6BN)···Cl(3)#4	0.82(4)	2.44(4)	3.222(3)	162(3)
N(5)−H(5BN)···Cl(3)	0.78(4)	2.46(4)	3.197(3)	160(4)
N(5)−H(5AN)···Cl(3)#3	0.87(4)	2.48(4)	3.280(3)	152(3)

[a] Symmetry transformations used to generate equivalent atoms: #1, $-x+1, y-{}^1/_2, -z+{}^1/_2$; #2, $x, -y+{}^3/_2, z-{}^1/_2$; #3, $-x, y-{}^1/_2, -z-{}^1/_2$; #4, $x, -y+{}^1/_2, z+{}^1/_2$.

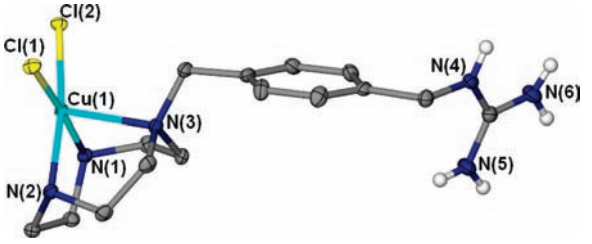

Figure 3. Thermal ellipsoid plot of the complex unit in **C3** showing the distorted SP copper(II) geometry (ellipsoids drawn at 50% probability; hydrogen atoms on carbon atoms, solvent molecules and counteranions have been omitted for clarity).

Table 3. Selected Bond Lengths [Å] and Angles [deg] for C3

Cu(1)−N(1)	2.012(1)	N(2)−Cu(1)−N(1)	83.35(5)
Cu(1)−N(2)	2.032(1)	N(1)−Cu(1)−Cl(2)	175.29(4)
Cu(1)−N(3)	2.283(1)	N(2)−Cu(1)−Cl(2)	92.01(4)
Cu(1)−Cl(1)	2.3199(4)	N(1)−Cu(1)−N(3)	82.48(4)
Cu(1)−Cl(2)	2.2741(4)	N(2)−Cu(1)−N(3)	82.72(4)
		Cl(2)−Cu(1)−N(3)	97.76(3)
		N(1)−Cu(1)−Cl(1)	90.74(4)
		N(2)−Cu(1)−Cl(1)	168.11(3)
		Cl(2)−Cu(1)−Cl(1)	93.69(1)
		N(3)−Cu(1)−Cl(1)	106.80(3)

Table 4. Hydrogen-Bonding Interactions in C3 [Å and deg][a]

D−H···A	d(D−H)	d(H···A)	d(D···A)	∠DHA
N(1)−H(1)···Cl(1)#1	0.83(2)	2.60(2)	3.321(1)	145.6(2)
N(5)−H(5NB)···Cl(3)	0.86(2)	2.40(2)	3.215(2)	158.1(2)
N(5)−H(5NA)···O(2)	0.83(2)	2.03(2)	2.810(2)	156.8(2)
N(6)−H(6NB)···Cl(3)	0.83(2)	2.48(2)	3.262(2)	156(2)
N(6)−H(6NA)···Cl(1)#2	0.83(2)	2.41(2)	3.218(2)	167.1(2)
O(2)−H(2O)···Cl(3)#3	0.82(2)	2.30(2)	3.114(1)	169.3(2)
O(1)−H(1O)···Cl(3)	0.84	2.30	3.141(1)	177.3

[a] Symmetry transformations used to generate equivalent atoms: #1, $-x, -y+1, -z$; #2, $-x, y+{}^1/_2, -z+{}^1/_2$; #3, $x, y-1, z$.

SP geometry and 100% for the ideal TBP geometry.[38] The τ value of 8% for **C1** indicates a geometry close to regular SP.

The mean deviation of the basal atoms from their least-squares plane is 0.036 Å, with a 0.19 Å out-of-plane displacement for copper(II), directed toward the apical nitrogen atom [N(3)]. As expected, the Cu−N distances in the basal plane are shorter than the Cu−N(apical) distance and the intraring N−Cu−N angles

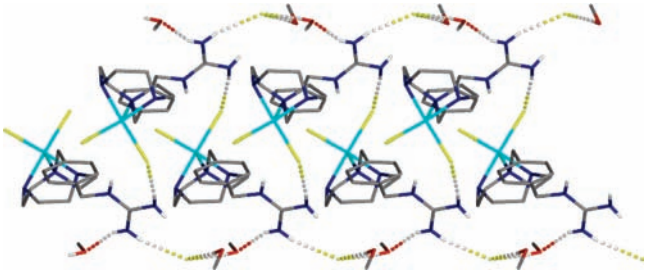

Figure 4. Stick representation showing a head-to-tail arrangement of the adjacent $[Cu(L^3H^+)Cl_2]^+$ units and the hydrogen bonding (dashed bonds) between the charged guanidinium arm, cocrystallized methanol molecules and chloride counteranions present in the crystal lattice of **C3**.

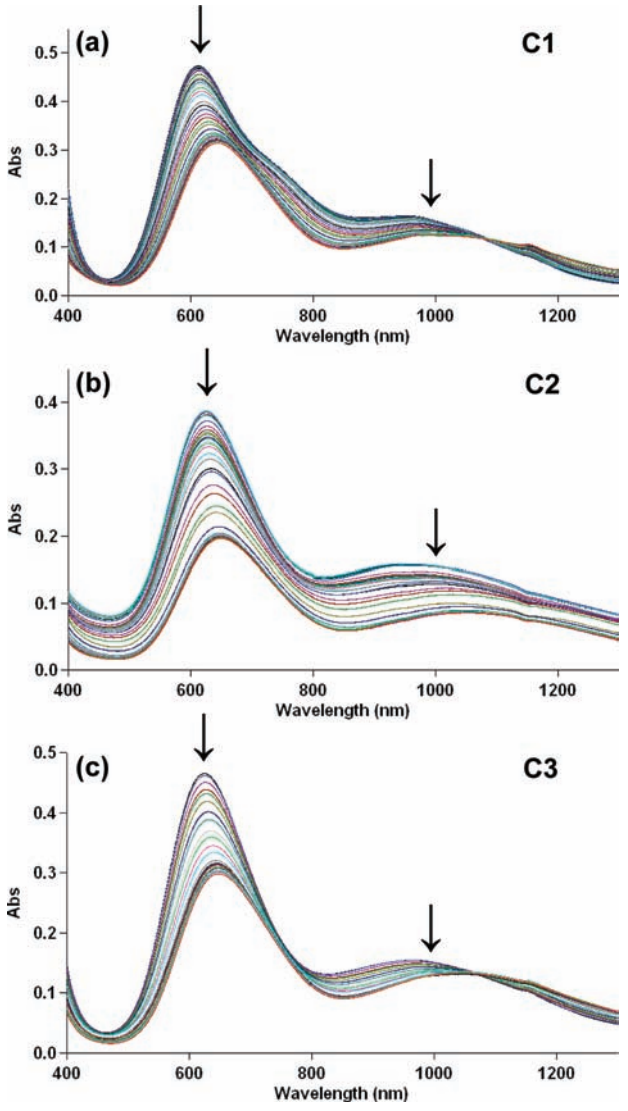

Figure 5. Change in the UV−vis−NIR spectrum of copper(II) complexes (7.5 mM) observed in the pH range 8.0−4.0. The top spectrum was recorded at pH 8.0 and the bottom spectrum at pH 4.0. Arrows indicate the decrease in the absorbance upon moving from pH 8 to 4.

dx.doi.org/10.1021/ic102301n |*Inorg. Chem.* 2011, 50, 4327–4339

are all <90° (Table 1). Coordination of the macrocycle also causes the Cu−N(apical) bond to be bent toward the basal plane. The Cu−N and Cu−Cl distances are similar to those measured for $[Cu(tacn)Cl_2]$.[37]

The protonated guanidinium group lies on the side of the aromatic ring opposite to the tacn macrocycle and is engaged in charge-assisted hydrogen bonding with the chloride counteranion and hydrogen bonds to the DMF molecule present in the lattice (Figure 2 and Table 2).

Table 5. Apparent pK_a Values of Coordinated Water Molecules in Copper(II) Complexes, Calculated from the Decrease in the Absorbance Intensities at Selected Wavelengths (i.e., 625, 900, and 1000 nm)

compound	pK_a (coordinated water)	ref
$[Cu(tacn)(OH_2)_2]^{2+}$	7.3	34
$[Cu(\mathbf{L^1})(OH_2)_2]^{2+}$ (**C1**)	6.36 ± 0.17	this work
$[Cu(\mathbf{L^2})(OH_2)_2]^{2+}$ (**C2**)	6.95 ± 0.18	this work
$[Cu(\mathbf{L^3})(OH_2)_2]^{2+}$ (**C3**)	7.08 ± 0.08	this work

Table 6. First-Order Rate Constants for Hydrolysis of BNPP by Copper(II) Complexes[a]

	k_{obs} ($\times 10^{-6}$ s^{-1})		
compound	pH 7.0	pH 9.0	ref
BNPP only	0.0003		this work
$[Cu(tacn)(OH_2)_2]^{2+}$	1.71 ± 0.01	6.3[31]	31
$[Cu(Bntacn)(OH_2)_2]^{2+}$	0.86 ± 0.05	2.55 ± 0.03	this work
$[Cu(\mathbf{L^1})(OH_2)_2]^{2+}$ (**C1**)	1.65 ± 0.03	3.07 ± 0.08	this work
$[Cu(\mathbf{L^2})(OH_2)_2]^{2+}$ (**C2**)	2.36 ± 0.03	7.02 ± 0.07	this work
$[Cu(\mathbf{L^3})(OH_2)_2]^{2+}$ (**C3**)	2.39 ± 0.04	7.49 ± 0.05	this work
$[Cu(\mathbf{A})]^{2+}$	0.0100 ± 0.0003		25
$[Cu(\mathbf{B})(OH_2)_2]^{2+}$	72.4 ± 0.8		25
$[Cu(Me_3tacn)(OH_2)]^{2+}$	37		31
$[Cu(^iPr_3tacn)(OH_2)]^{2+}$	43		41

[a] Conditions: [complex] = 2 mM, [BNPP] = 0.1 mM, [HEPES] or [CHES] = 50 mM, [I] = 0.15 M, and T = 50 °C). Abbreviations: Bntacn = 1-benzyl-1,4,7-triazacyclononane, **A** = 1-ethyl-4,7-bis(2-guanidinoethyl)-1,4,7-triazacyclononane, **B** = 1-ethyl-4,7-bis(3-guanidinopropyl)-1,4,7-triazacyclononane, Me_3tacn = 1,4,7-trimethyl-1,4,7-triazacyclononane and $^iPr_3$tacn = 1,4,7-triisopropyl-1,4,7-triazacyclononane.

Complex ***C3***. The crystal structure of **C3** is composed of discrete cationic $[Cu(\mathbf{L^3}H^+)Cl_2]^+$ units (Figure 3) and non-coordinated chloride anions and methanol molecules. The copper(II) center resides in a distorted SP environment, with the degree of distortion from the ideal SP geometry measured as τ = 12%.[38] The Cu−N distances and angles describing coordination of $\mathbf{L^3}$ to the copper(II) center are almost identical to those observed in **C1** (Table 3).

The halide ligand Cl(1) with the longer Cu−Cl bond distance participates in intermolecular hydrogen bonding with the protonated guanidinium group of an adjacent complex unit (Table 4). This results in a head-to-tail arrangement of the $[Cu(\mathbf{L^3}H^+)Cl_2]^+$ units within the crystal lattice of **C3**. In addition, hydrogen-bonding interactions between the guanidinium groups, the cocrystallized methanol molecules, and chloride counteranions link the alternate guanidinium pendants to each other (Figure 4).

Solution Speciation Studies. To investigate the acid−base properties of complexes **C1**−**C3**, a series of spectrophotometric pH titrations were carried out that monitored changes in the electronic spectrum of each complex as a function of the pH (see Figure 5). Analysis of the systematic decrease in the absorbance as the pH was decreased from 8.0 to 4.0 allowed determination of the apparent pK_a of the coordinated water molecules (see Figures S01−S03 in the Supporting Information and Table 5). **C2** and **C3** were found to have pK_a values of ca. 7, close to that previously measured for the nonfunctionalized Cu^{II}tacn complex,[34] while that for **C1** is substantially lower (6.4), indicating that the coordinated water molecule in this complex is significantly more acidic. This could be due to the closer proximity of the charged guanidine pendant in **C1**, inductively lowering the pK_a of the coordinated water, as previously proposed for related complexes with guanidinium pendants.[39,40]

Cleavage of Model Phosphodiesters. The rates of cleavage of the simple model phosphodiesters BNPP and HPNPP by complexes **C1**−**C3** were measured at a series of different pH values, together with those of the nonguanidinium analogues, $[Cu(Bntacn)(OH_2)_2]^{2+}$ and $[Cu(tacn)(OH_2)_2]^{2+}$ (Tables 6 and 7). At all pHs and for both substrates, each of the complexes enhanced the rate of cleavage significantly above background levels, particularly for the less reactive DNA mimic, BNPP (HPNPP, like RNA, features a 2′-OH group on the ribose ring that may act as an internal nucleophile). In addition, the cleavage activity increased with the pH in each case, consistent with the

Table 7. First-Order Rate Constants for Hydrolysis of HPNPP by Copper(II) Complexes[a]

	k_{obs} ($\times 10^{-6}$ s^{-1})			
compound	pH 6.0	pH 7.0	pH 9.0	ref
HPNPP[b] only	0.019	0.012 ± 0.007	0.807	this work
$[Cu(tacn)(OH_2)_2]^{2+}$[b]	0.037	3.58 ± 0.2	8.69	this work
$[Cu(Bntacn)(OH_2)_2]^{2+}$	0.086 ± 0.0002	1.73 ± 0.02	2.63 ± 0.05	this work
$[Cu(\mathbf{L^1})(OH_2)_2]^{2+}$ (**C1**)	0.754 ± 0.007	1.88 ± 0.03	3.27 ± 0.09	this work
$[Cu(\mathbf{L^2})(OH_2)_2]^{2+}$ (**C2**)	1.51 ± 0.02	2.74 ± 0.02	10.1 ± 0.6	this work
$[Cu(\mathbf{L^3})(OH_2)_2]^{2+}$ (**C3**)	0.936 ± 0.006	2.30 ± 0.03	9.55 ± 0.01	This work
$[Cu(\mathbf{A})]^{2+}$[b]		0.13 ± 0.06		25
$[Cu(\mathbf{B})(OH_2)_2]^{2+}$		32.0 ± 3		25

[a] Conditions: [complex] = 2 mM, [HPNPP] = 0.1 mM [MES], [HEPES] or [CHES] = 50 mM, [I] = 0.15 M, and T = 25 °C). Abbreviations: Bntacn = 1-benzyl-1,4,7-triazacyclononane, **A** = 1-ethyl-4,7-bis(2-guanidinoethyl)-1,4,7-triazacyclononane and **B** = 1-ethyl-4,7-bis(3-guanidinopropyl)-1,4,7-triazacyclononane. [b] Data were analyzed using the initial rate method, yielding k_{obs} directly.

dx.doi.org/10.1021/ic102301n |*Inorg. Chem.* 2011, 50, 4327–4339

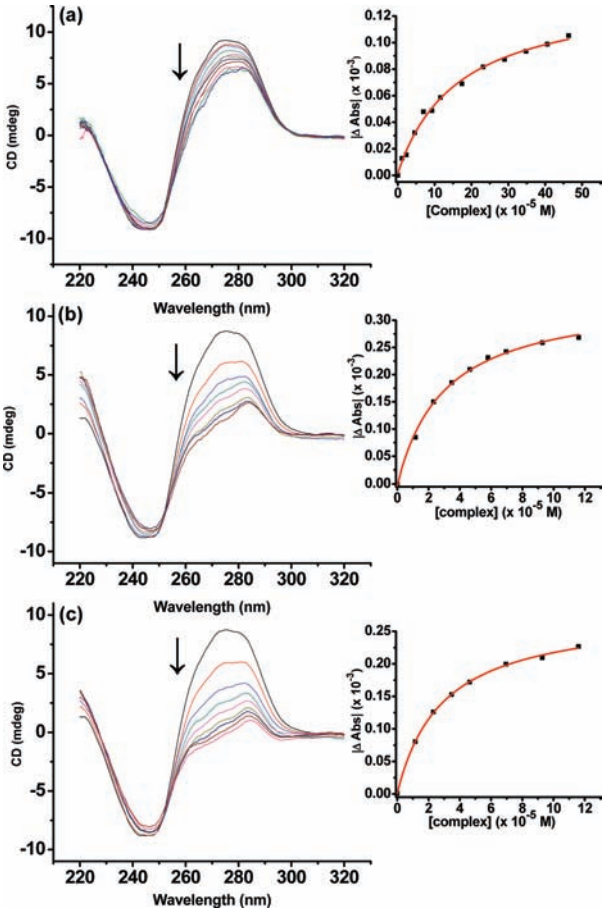

Figure 6. CD spectra for CT-DNA in the presence of increasing amounts of copper(II) complexes, **C1**−**C3** (a−c). Conditions: [complex]/[DNA] = 0.0, 0.1, 0.2, 0.4, 0.6, 0.8, 1.0, 1.5, 2.0, 2.5, 3.0, 3.5 and 4.0), and [CT-DNA] = 0.116 mM in 5 mM Tris-HCl/50 mM NaCl buffer. Arrows indicate the decrease in the 275 nm band with increasing amounts of complexes. Insets show the change in the absorbance at the initial peak maximum with increasing concentrations of complexes.

postulated hydrolytic mechanism for Cu^{II}tacn-based complexes, which features a copper(II)-bound hydroxide nucleophile as the active species.[7] At neutral or basic pH, the rates of phosphodiester cleavage by the three complexes were similar to those for $[Cu(Bntacn)(OH_2)_2]^{2+}$ and $[Cu(tacn)(OH_2)_2]^{2+}$, suggesting that the guanidinium groups do not directly interact with the phosphodiester groups and/or are not active participants in the cleavage mechanism. At pH 6, the complexes were found to be substantially more reactive toward HPNPP than either $[Cu(tacn)(OH_2)_2]^{2+}$ or $[Cu(Bntacn)(OH_2)_2]^{2+}$, suggesting some contribution from the guanidinium groups toward the cleavage activity at this particular pH.

The cleavage activities of complexes **C1**−**C3** are substantially lower than those measured previously at pH 7 for the analogue featuring two propylguanidine pendants, as well as the copper complexes of the simple N-alkylated tacn ligands (also listed in Tables 6 and 7). For these latter systems, the enhanced activity relative to $[Cu(tacn)(OH_2)_2]^{2+}$ has been ascribed to the N-linked substituents inhibiting the formation of inactive dihydroxo-bridged dimers. This suggests that the single pendants in **C1**−**C3** may be relatively ineffectual at inhibiting the formation of such dimers at pH 7.

Table 8. Apparent Binding Constants for Interaction of Copper(II) Complexes with CT-DNA in 5 mM Tris-HCl/50 mM NaCl Buffer (pH 7.0)

compound	K_b ($\times 10^3$ M^{-1})
$[Cu(\mathbf{L}^1)(OH_2)_2]^{2+}$ (**C1**)	6.09 ± 0.70
$[Cu(\mathbf{L}^2)(OH_2)_2]^{2+}$ (**C2**)	33.0 ± 2.8
$[Cu(\mathbf{L}^3)(OH_2)_2]^{2+}$ (**C3**)	34.5 ± 1.7

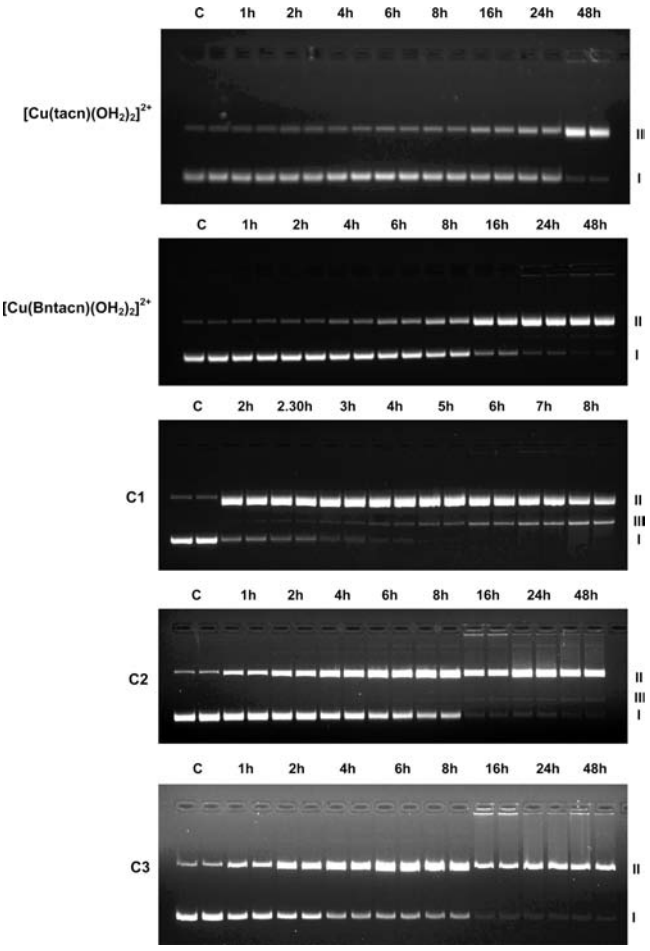

Figure 7. Agarose gel images showing cleavage of pBR 322 plasmid DNA (38 μM bp) incubated with $[Cu(tacn)(OH_2)_2]^{2+}$, $[Cu(Bntacn)(OH_2)_2]^{2+}$ and **C1**−**C3** (150 μM) in a HEPES buffer (40 mM, pH 7.0) at 37 °C for various time intervals. C = DNA control.

Interaction of Complexes with DNA. CD spectroscopy is a useful technique for monitoring changes in the DNA conformation in solution and provides information about binding interactions with DNA. Free helical DNA exhibits the so-called right-handed B form CD spectrum, with a positive band at 275 nm due to base stacking and a negative band at 245 nm due to helicity.[42] Changes in the CD signals of DNA observed upon interaction with small molecules have often been assigned to the corresponding changes in the DNA structure.[43,44] The intercalation of small molecules to DNA is known to stabilize the right-handed B conformation of CT-DNA, resulting in an increase in the intensities of both bands. In contrast, electrostatic interactions between small molecules with DNA generally result in little or no change in the intensities of the two bands.[45] Titration of complex

dx.doi.org/10.1021/ic102301n |*Inorg. Chem.* 2011, 50, 4327–4339

Table 9. Observed Rate Constants for Single-Strand Cleavage of pBR 322 Plasmid DNA by Copper(II) Complexes[a]

compound	k_{obs} ($\times 10^{-5}$ s^{-1})	ref
$[Cu(tacn)(OH_2)_2]^{2+}$	1.2 ± 0.4	25
$[Cu(tacn)(OH_2)_2]^{2+}$[b]	1.5	34
$[Cu(Bntacn)(OH_2)_2]^{2+}$	2.2 ± 0.5	this work
$[Cu(\mathbf{L^1})(OH_2)_2]^{2+}$ (**C1**)	k_1 = 27 ± 3	this work
	k_2 = 1.2 ± 0.5	
	k_3 = 11.2 ± 0.5	
$[Cu(\mathbf{L^2})(OH_2)_2]^{2+}$ (**C2**)	8.2 ± 1.0	this work
$[Cu(\mathbf{L^3})(OH_2)_2]^{2+}$ (**C3**)	6.7 ± 0.3	this work
$[Cu(\mathbf{A})]^{2+}$	1.58 ± 0.05	25
$[Cu(\mathbf{B})(OH_2)_2]^{2+}$	2.53 ± 0.04	25
$[Cu(^{i}Pr_3tacn)(OH_2)]^{2+}$[b]	3.0	34, 41
$[Cu(TACI)(OH_2)_2]^{2+}$[c]	k_1 = 230	47
	k_2 = 6.2	
$[Cu(\mathbf{C})(OH_2)_2]^{2+}$[d]	85	48

[a] Conditions: [complex] = 150 μM, [pBR 322 plasmid] = 38 μM bp, [HEPES] = 40 mM (pH 7.0 at 37 °C). Abbreviations: Bntacn = 1-benzyl-1,4,7-triazacyclononane, **A** = 1-ethyl-4,7-*bis*(2-guanidinoethyl)-1,4,7-triazacyclononane, **B** = 1-ethyl-4,7-bis(3-guanidinopropyl)-1,4,7-triazacyclononane, $^{i}Pr_3tacn$ = 1,4,7-triisopropyl-1,4,7-triazacyclononane, TACI = *all-cis*-2,4,6-triamino-1,3,5-trihydroxycyclohexane and **C** = 5,5′-bis(guanidinomethyl)-2,2′-bipyridyl. [b] [complex] = 25 μM, [pBluescript II ks(−) supercoiled] = 25 nM bp at 50 °C, pH 7.8. [c] [complex] = 48 μM, [pBR 322 plasmid] = 12 μM bp at 37 °C, pH 8.1. [d] [complex] = 150 μM, [pBR 322 plasmid] = 38 μM bp at 37 °C, pH 7.2.

C1 into CT-DNA induced a slight decrease in the intensity of the band at 275 nm (Figure 6). For complexes **C2** and **C3**, however, more pronounced reductions in the intensity were observed, suggesting a greater degree of distortion of the initial DNA structure. The apparent binding constants determined for each complex (as indicated in the Experimental Section) are summarized in Table 8. Significantly higher K_b values were found for complexes **C2** and **C3** compared to **C1**. This difference in affinity can be ascribed to differences in the charge of the complexes; viz., **C1** is predominantly deprotonated at pH 7.0 (2+ charge, pK_a = 6.36), whereas **C2** and **C3** exist as a roughly equimolar mixture of protonated and deprotonated forms at this pH.

Cleavage of Plasmid DNA. The ability of complexes **C1**−**C3** to cleave DNA was assessed by incubating them with plasmid pBR 322 DNA under physiological conditions (i.e., pH 7.0 and T = 37 °C). Conversion of the supercoiled form (form I) of the DNA to the nicked circular form (form II) and linear form (form III) was monitored by gel electrophoresis (Figure 7). In each case, a decrease in the intensity of the band due to form I with the incubation time was accompanied by the appearance and intensification of a band corresponding to form II of the plasmid DNA (as well as form III in the case of **C1**). Control experiments revealed that no measurable DNA cleavage occurred when pBR 322 plasmid DNA was incubated with either 150 μM of the nonmetalated ligands or 150 μM $CuCl_2$ (Figure S22 in the Supporting Information), clearly indicating that the observed cleavage was due to the metal complexes. Experiments carried out at variable concentrations of each complex revealed a maximum rate of DNA cleavage at a concentration of 150 μM (for typical DNA electrophoresis gels see Figures S04−S06 and Table S02 in the Supporting Information). The lower cleavage rates observed above this concentration may be due to the

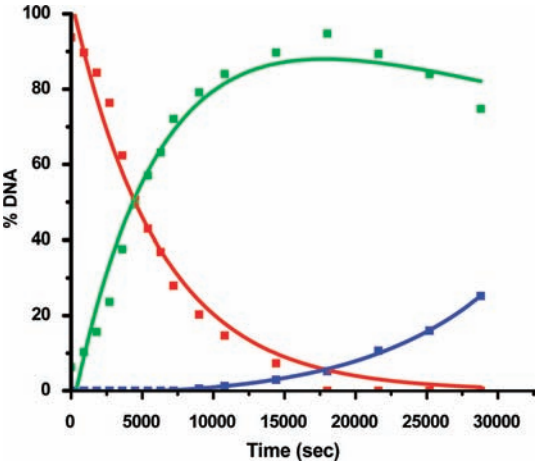

Figure 8. Time course showing conversion of the supercoiled form (red) of pBR322 plasmid DNA to the nicked (green) and linear (blue) forms in the presence of **C1**. The solid lines show the fit of the experimental data (squares) to the single-strand cleavage model of Kishikawa et al.[33]

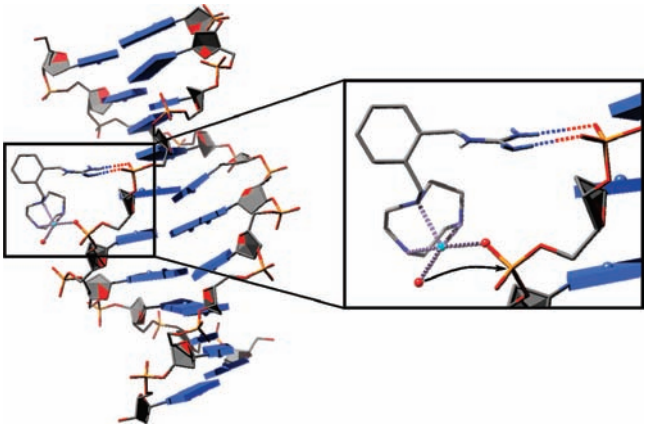

Figure 9. Stick model showing the plausible mode of interaction between complex **C1** and DNA and the subsequent attack of a copper(II)-bound hydroxide nucleophile on a phosphodiester linkage. Charge-assisted hydrogen bonding between the protonated guanidine and phosphate backbone is represented by dashed bonds (stick model for the B-DNA duplex generated using the PDB entry: 3IXN, using the UCSF Chimera Software Package).[49]

increased formation of dihydroxo-bridged dimers, which bind to the DNA through electrostatic interactions and block access of the cleavage-active monomeric species.[31,32,41,46] A predominantly hydrolytic (as opposed to redox-mediated) mode of cleavage was confirmed through experiments performed in the presence of various scavengers for reactive oxygen species (Figures S13−S18 in the Supporting Information), as well as under anaerobic conditions (Figures S19−S21 in the Supporting Information), consistent with earlier observations for other Cu^{II}tacn-based complexes.[25,34]

For all of the complexes except **C1**, the DNA cleavage data were satisfactorily fitted to a first-order expression, yielding the first-order rate constant k_{obs} for cleavage of form I DNA to produce form II (Table 9). A single-strand cleavage model derived by Kishikawa et al.[33] was used to fit the kinetic profiles for **C1**. This model accounts for not only the conversion of form I

dx.doi.org/10.1021/ic102301n |*Inorg. Chem.* 2011, 50, 4327–4339

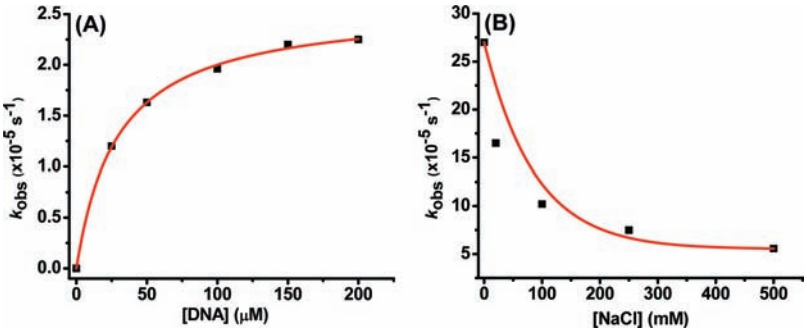

Figure 10. (A) Saturation kinetics of pBR 322 DNA cleavage using 50 μM **C1** with different concentrations of pBR 322 DNA (25−200 μM) at 37 °C in a 40 mM HEPES buffer (pH 7.0). (B) Ionic strength dependence profile for DNA cleavage promoted by 150 μM **C1** in the presence of different concentrations of NaCl (0, 20, 100, 250, and 500 mM). The lines show the general data trends only.

to form II (k_1) but also the subsequent nicking of form II to produce form III (k_2) and further cleavage of form III to produce undetected forms of DNA (k_3; see the Experimental Section for rate equations). Figure 8 shows the best fit of the experimental cleavage data for **C1**, with the corresponding values of k_1, k_2, and k_3 reported in Table 9.

The greater rates of DNA cleavage observed in the presence of complexes **C1**−**C3** compared to the nonguanidinium analogues, $[Cu(Bntacn)(OH_2)_2]^{2+}$ and $[Cu(tacn)(OH_2)_2]^{2+}$, contrast dramatically with the findings for the BNPP and HPNPP substrates. This is especially the case for **C1**, which was found to cleave BNPP and HPNPP at rates similar to $[Cu(tacn)(OH_2)_2]^{2+}$, whereas plasmid DNA cleavage was ca. 22-fold faster. These results indicate that the enhanced nuclease activity of **C1**−**C3** could be due to them having greater affinity for plasmid DNA than the nonguanidinylated complexes. This conclusion is supported by the fact that these complexes were shown to bind strongly to CT-DNA (vide supra). In this context, the charged guanidinium pendants interact with neighboring phosphodiester groups in the DNA backbone rather than acting in concert with the copper(II) center to activate the phosphodiester linkage undergoing cleavage. We note that it is possible to position the X-ray crystal structure of **C1** next to a DNA double helix such that the guanidinium group forms strong charge-assisted hydrogen bonds with a phosphodiester group, while the copper(II) center coordinates to the oxygen atom of an adjacent phosphodiester, with a cis-disposed hydroxo ligand well-poised to carry out nucleophilic attack on the phosphorus atom (Figure 9). The significantly higher activity of **C1** compared to **C2** and **C3** can also be partly rationalized in terms of the greater acidity of this complex (pK_a = 6.4 compared to 7.0 for **C2** and **C3**), which means that, under the conditions used for the DNA cleavage experiments, a higher concentration of the conjugate base, $[Cu(\mathbf{L^1}H^+)(OH)(OH_2)]^{2+}$, would be present, leading to a faster rate of cleavage.

In order to help assess whether the enhanced reactivity of the guanidinium-bearing complexes toward DNA was a reflection of enhanced binding, we examined the dependence of the cleavage activity on the substrate concentration and ionic strength (for complex **C1** only). Cleavage experiments performed using a constant **C1** complex concentration (50 μM) and variable DNA concentration (25−200 μM; Figures 10A and S10 in the Supporting Information) revealed the expected increase in the observed cleavage rate with increasing DNA concentration, while increasing ionic strength (adjusted by adding NaCl) was found to decrease the DNA cleavage reactivity (Figures 10B and S11 in the Supporting Information), consistent with a "quenching" of electrostatic interactions between $[Cu(\mathbf{L^1}H^+)(OH)(OH_2)]^{2+}$ (the predominant form of **C1** existing at pH 7.0) and the negatively charged phosphate backbone of DNA. Furthermore, variation of $\log(k_{obs})$ with $I^{1/2}$, where I = ionic strength, was found to be linear (Figure S12 in the Supporting Information), indicative of a bimolecular reaction between charged reactants.

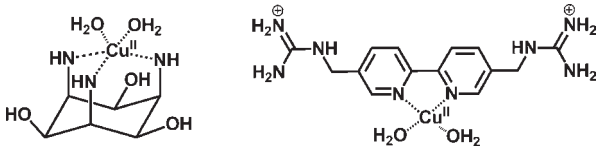

Figure 11. Examples of copper(II) complexes exhibiting higher nuclease activity than **C1**.[47,48]

Complex **C1** exhibits the fastest rate of plasmid DNA cleavage within the family of Cu^{II}tacn complexes reported so far.[25,34] It is considerably more active than the analogues featuring two alkylguanidine pendants, as well as the copper complexes of simple N-alkylated tacn ligands (Table 9). However, more active synthetic nucleases have been reported, such as the copper(II) complexes of *all-cis*-2,4,6-triamino-1,3,5-trihydroxycyclohexane (TACI)[47] and a 2,2′-bipyridine derivative featuring guanidinium substituents[48] (Figure 11), which are 3 and 9 times more active than **C1**, respectively (Table 9; it should be noted, however, that the activity of the TACI complex was measured at pH 8.1). For both of these complexes, secondary interactions between ancillary groups and the DNA backbone have also been shown to make an important contribution to the observed cleavage activity. Their higher reactivities compared to that of **C1** are likely to reflect an enhanced capacity of the copper(II) centers to access the sugar−phosphate backbone of the plasmid DNA because the supporting ligand structures are less sterically demanding than that in **C1**. The better DNA cleavage properties of the Cu^{II}TACI complex also extends to conversion of the relaxed circular DNA to linear DNA, with the reported k_2 value being 5-fold higher than that determined here for **C1**.

CONCLUSION

Attachment of *o*-, *m*-, and *p*-xylylguanidinium pendants to the tacn macrocycle results in copper(II) complexes with enhanced nuclease activity compared to the "control" compounds, $[Cu(Bntacn)(OH_2)_2]^{2+}$ and $[Cu(tacn)(OH_2)_2]^{2+}$. However,

dx.doi.org/10.1021/ic102301n |*Inorg. Chem.* 2011, 50, 4327–4339

the complexes are no more reactive toward the model compounds, BNPP and HPNPP, containing single phosphodiester linkages, which indicates that the guanidinium groups most likely do not interact directly with the phosphodiester group undergoing cleavage but rather enhance the concentration of the complex in the vicinity of plasmid DNA by forming favorable interactions with an adjacent phosphodiester group. For the complex of the *o*-xylyl derivative (**C1**), a greater cleavage activity compared to those of the *m*- and *p*-xylyl derivatives (**C2** and **C3**) can be ascribed to the higher acidity of coordinated water, which generates a higher concentration of the deprotonated complex involved in hydrolysis at neutral pH. This study further highlights the potential to improve the activity of simple model systems through the introduction of charged auxiliary groups but indicates that a more rigid positioning of the guanidine group is desirable to better mimic the cooperativity between metal ions and arginine residues that occurs within the active sites of many metallonucleases.

■ ASSOCIATED CONTENT

Supporting Information. Crystallographic files in CIF format, table of crystallographic data (Table S01), absorbance versus $[H^+]$ graphs for solutions of Cu(II) complexes (Figures S01−S03), agarose gel images of DNA cleavage and kinetic profiles (Figures S04−S22 and Tables S02−S11), and graphs showing the extent of DNA cleavage in the presence of scavenging agents and under aerobic/anaerobic conditions (Figures S14, S16, S18, and S23). This material is available free of charge via the Internet at http://pubs.acs.org.

■ AUTHOR INFORMATION

Corresponding Author

*E-mail: Bim.Graham@monash.edu. (B.G.), Leone.Spiccia@monash.edu (L.S.). Fax: +61 3 9903 9582 (B.G.), +61 3 9905 4597 (L.S.).

Present Addresses

‡School of Chemistry, Ruprecht-Karls-Universität, Heidelberg, Germany.

■ ACKNOWLEDGMENT

This work was supported by the Australian Research Council through the Discovery Program. L.T. is the recipient of a Monash Graduate Scholarship and Postgraduate Publication Award.

■ REFERENCES

(1) Jiang, Q.; Xiao, N.; Shi, P. F.; Zhu, Y. G.; Guo, Z. J. *Coord. Chem. Rev.* **2007**, *251*, 1951–1972.
(2) Mancin, F.; Scrimin, P.; Tecilla, P.; Tonellato, U. *Chem. Commun.* **2005**, 2540–2548.
(3) Suh, J. *Acc. Chem. Res.* **2003**, *36*, 562–570.
(4) Sreedhara, A.; Cowan, J. A. *J. Biol. Inorg. Chem.* **2001**, *6*, 337–347.
(5) Cowan, J. A. *Chem. Rev.* **1998**, *98*, 1067–1088.
(6) Williams, N. H.; Takasaki, B.; Wall, M.; Chin, J. *Acc. Chem. Res.* **1999**, *32*, 485–493.
(7) Hegg, E. L.; Burstyn, J. N. *Coord. Chem. Rev.* **1998**, *173*, 133–165.
(8) Burrows, C. J.; Muller, J. G. *Chem. Rev.* **1998**, *98*, 1109–1152.
(9) Pogozelski, W. K.; Tullius, T. D. *Chem. Rev.* **1998**, *98*, 1089–1108.
(10) Breaker, R. R. *Chem. Rev.* **1997**, *97*, 371–390.
(11) Wilcox, D. E. *Chem. Rev.* **1996**, *96*, 2435–2458.
(12) Sigman, D. S.; Mazumder, A.; Perrin, D. M. *Chem. Rev.* **1993**, *93*, 2295–2316.
(13) Dixon, M.; Webb, E. C. *Enzymes*; 3rd ed.; Academic Press: New York, 1979.
(14) Trawick, B. N.; Daniher, A. T.; Bashkin, J. K. *Chem. Rev.* **1998**, *98*, 939–960.
(15) Gani, D.; Wilkie, J. *Structure Bonding (Berlin)*; Springer: Berlin/Heidelberg, 1997.
(16) Strater, N.; Lipscomb, W. N.; Klabunde, T.; Krebs, B. *Angew. Chem., Int. Ed. Engl.* **1996**, *35*, 2024–2055.
(17) An, Y.; Tong, M.-L.; Ji, L.-N.; Mao, Z.-W. *Dalton Trans.* **2006**, 2066–2071.
(18) Kovari, E.; Heitker, J.; Kramer, R. *J. Chem. Soc., Chem. Commun.* **1995**, 1205–1206.
(19) Kovari, E.; Kramer, R. *J. Am. Chem. Soc.* **1996**, *118*, 12704–12709.
(20) Jubian, V.; Dixon, R. P.; Hamilton, A. D. *J. Am. Chem. Soc.* **1992**, *114*, 1120–1121.
(21) Dixon, R. P.; Geib, S. J.; Hamilton, A. D. *J. Am. Chem. Soc.* **1992**, *114*, 365–366.
(22) Cotton, F. A.; Hazen, E. E. J.; Legg, M. *Proc. Natl. Acad. Sci. U.S. A.* **1979**, *76*, 2551–2555.
(23) Weber, D. J.; Meeker, A. K.; Mildvan, A. S. *Biochemistry* **1991**, *30*, 6103–6114.
(24) Christianson, D. W.; Lipscomb, W. N. *Acc. Chem. Res.* **1989**, *22*, 62–69.
(25) Tjioe, L.; Joshi, T.; Brugger, J.; Graham, B.; Spiccia, L. *Inorg. Chem.* **2011**, *50*, 621–635.
(26) Kaminskaia, N. V.; He, C.; Lippard, S. J. *Inorg. Chem.* **2000**, *39*, 3365–3373.
(27) Sissi, C.; Rossi, P.; Felluga, F.; Formaggio, F.; Palumbo, M.; Tecilla, P.; Toniolo, C.; Scrimin, P. *J. Am. Chem. Soc.* **2001**, *123*, 3169–3170.
(28) Kimura, S.; Bill, E.; Bothe, E.; Weyhermuller, T.; Wieghardt, K. *J. Am. Chem. Soc.* **2001**, *123*, 6025–6039.
(29) Brown, D. M.; Usher, D. A. *J. Chem. Soc.* **1965**, 6558–6564.
(30) Tsang, J. S.; Neverov, A. A.; Brown, R. S. *J. Am. Chem. Soc.* **2003**, *125*, 1559–1566.
(31) Fry, F.; Fischmann, A. J.; Belousoff, M. J.; Spiccia, L.; Brugger, J. *Inorg. Chem.* **2005**, *44*, 941–950.
(32) Belousoff, M. J.; Duriska, M. B.; Graham, B.; Batten, S. R.; Moubaraki, B.; Murray, K. S.; Spiccia, L. *Inorg. Chem.* **2006**, *47*, 3746–3755.
(33) Kishikawa, H.; Jiang, Y.-P.; Goodisman, J.; Dabrowiak, J. C. *J. Am. Chem. Soc.* **1991**, *113*, 5434–5440.
(34) Hegg, E. L.; Burstyn, J. N. *Inorg. Chem.* **1996**, *35*, 7474–7481.
(35) Sheldrick, G. M. *SHELXL-97*; University of Gottingen: Gottingen, Germany, 1997.
(36) Sheldrick, G. M. *SHELXS-97*; University of Gottingen: Gottingen, Germany, 1997.
(37) Schwindinger, W. F.; Fawcett, T. G.; Lalancette, R. A.; Potenza, J. A.; Schugar, H. J. *Inorg. Chem.* **1980**, *19*, 1379–1381.
(38) Addison, A. W.; Rao, T. N.; Reedjik, J.; Rijin, J. V.; Verschoor, G. C. *J. Chem. Soc., Dalton Trans.* **1984**, 1349–1356.
(39) Aoki, S.; Iwaida, K.; Hanamoto, N.; Shiro, M.; Kimura, E. *J. Am. Chem. Soc.* **2002**, *124*, 5256–5257.
(40) Belousoff, M. J.; Tjioe, L.; Graham, B.; Spiccia, L. *Inorg. Chem.* **2008**, *47*, 8641–8651.
(41) Deck, K. M.; Tseng, T. A.; Burstyn, J. N. *Inorg. Chem.* **2002**, *41*, 669–677.
(42) Collins, J. G.; Shields, T. P.; Barton, J. K. *J. Am. Chem. Soc.* **1994**, *116*, 9840–9846.
(43) Richards, A. D.; Rodger, A. *Chem. Soc. Rev.* **2007**, *36*, 471–483.
(44) Li, D.-D.; Huang, F.-P.; Chen, G.-J.; Gao, C.-Y.; Tian, J.-L.; Gu, W.; Liu, X.; Yan, S.-P. *J. Inorg. Biochem.* **2010**, *104*, 431–441.
(45) Uma Maheswari, P.; Palaniandavar, M. *J. Inorg. Biochem.* **2004**, *98*, 219–230.

(46) Belousoff, M. J.; Battle, A. R.; Graham, B.; Spiccia, L. *Polyhedron* **2007**, *26*, 344–355.
(47) Sissi, C.; Mancin, F.; Gatos, M.; Palumbo, M.; Tecilla, P.; Tonellato, U. *Inorg. Chem.* **2005**, *44*, 2310–2317.
(48) He, J.; Hu, P.; Wang, Y. J.; Tong, M.-L.; Sun, H. Z.; Mao, Z.-W.; Ji, L.-N. *Dalton Trans.* **2008**, 3207–3214.
(49) Pettersen, E. F.; Goddard, T. D.; Huang, C. C.; Couch, G. S.; Greenblatt, D. M.; Meng, E. C.; Ferrin, T. E. *J. Comput. Chem.* **2004**, *25*, 1605–1612.